Green Chemistry

PAPER

View Article Online
View Journal | View Issue

Cite this: *Green Chem.*, 2025, **27**, 10875

Spider web-inspired gelatin-based bioplastic enables closed-loop recyclable, biodegradable, and sustainable packaging

Yuehong Zhang,*[a,b,c] Langlang Dai,[a,c] Chen Yang,[a,c] Bin Wei[a,c] and Guangfu Liao *[d]

We present a spider web-inspired gelatin (GE) bioplastic engineered by the integration of natural tea polyphenols (TP), gelatin, and bio-based hyperbranched polyester (HBPE) synthesized from glycerol and itaconic anhydride. The resulting TP-HBPE-GE exhibits multifunctionality, including balanced optical properties for food packaging (52% visible light transmission and 99.8% UV blocking), a mechanically tunable biomimetic network enabling glycerol-free customization of strength and toughness (11.0–33.8 MPa tensile strength and 21.6%–125.3% elongation at break), dual moisture resistance combining hydrophobic surfaces (113.3° contact angle) and low vapor permeability with high barrier properties (803.1 g $(m^2\ day)^{-1}$), and bioactive preservation through antioxidant (88.6% DPPH scavenging) and antimicrobial actions (complete eradication of *E. coli* and *S. aureus*). Practical validation demonstrates superior cherry tomato preservation compared to commercial polyvinyl chloride (PVC), maintaining firmness and retaining nutrients over 15 days. The system embodies circular design principles through its renewable composition (gelatin, TP and HBPE), energy-efficient processing (water-based fabrication and thermal remodeling), closed-loop recyclability (conversion to adhesives/coatings), and full biodegradation within 28 days. This architecturally engineered bioplastic establishes a sustainable packaging paradigm aligned with green chemistry principles, including prioritization of renewable feedstocks, minimized process environmental footprints, valorization of waste films as adhesives and coatings, and ensured end-of-life biodegradability.

Received 9th June 2025,
Accepted 1st August 2025

DOI: 10.1039/d5gc02900g

rsc.li/greenchem

Green foundation

1. This work developed a bio-inspired strategy to fabricate sustainable gelatin-based bioplastics by utilizing renewable feedstocks, energy-efficient processing, and waste valorization, while minimizing hazards. This approach establishes a closed-loop lifecycle from production to degradation.
2. Employing a dual-network strategy simultaneously enhances the strength and toughness of gelatin-based bioplastics. These bioplastic films outperform commercial PVC in preserving cherry tomatoes, retaining firmness and nutrients for over 15 days. Importantly, the waste material derived from the films is convertible into high-value adhesives and coatings, underpinning a sustainable lifecycle.
3. Future research will focus on validating real-world degradation by testing biodegradation in diverse natural environments, as well as expanding functionality and scale through large-scale production while maintaining material properties.

1. Introduction

Plastic films are indispensable in modern packaging, construction, and agriculture due to their durability and cost-effectiveness.[1,2] However, the production and waste disposal of conventional plastic films violate green chemistry principles, primarily through their reliance on non-renewable feedstocks, generation of persistent non-degradable waste, and energy-intensive manufacturing processes.[3] These challenges necessitate the development of sustainable alternatives that combine renewable feedstocks with enhanced environmental performance while meeting practical perform-

[a]*College of Bioresources Chemical and Materials Engineering, Shaanxi University of Science and Technology, Xi'an 710021, China. E-mail: yuehong.zhang@sust.edu.cn*
[b]*School of Chemical Engineering and Technology, Tianjin University, Tianjin 300072, China*
[c]*Xi'an Key Laboratory of Green Chemicals and Functional Materials, Xi'an 710021, China*
[d]*National Forestry and Grassland Administration Key Laboratory of Plant Fiber Functional Materials, College of Materials Engineering, Fujian Agriculture and Forestry University, Fuzhou 350002, China. E-mail: liaogf@mail2.sysu.edu.cn*

ance requirements. Natural polymers such as cellulose,[4] chitosan,[5] and starch[6] show significant potential as bioplastic precursors due to their biodegradability and abundance. Similarly, researchers have explored bio-based monomers derived from natural polymers to synthesize high-performance bioplastics. For example, Sha *et al.*[7] synthesized a renewable, chemically recyclable polymer using starch-derived isomannide. Nevertheless, both natural polymers and their derivatives often suffer from poor processability in high-solid aqueous systems and typically require energy-intensive or solvent-based methods.

In contrast, gelatin (GE), a collagen-derived protein, aligns with green chemistry principles through waste valorization. It possesses inherent advantages as a promising candidate for bioplastic fabrication, including facile formation of high-solid-content aqueous solutions, complete biodegradability, and abundant availability.[8,9] Nevertheless, unmodified GE films lack sufficient mechanical robustness and functional versatility for practical applications.[10]

Common modification strategies, such as chemical crosslinking,[11] blending,[12] and nanofiller reinforcement,[13] have been used to improve the properties of gelatin-based bioplastic films. For instance, Chen *et al.*[14] modified gelatin using sulfonated fish oil as a plasticizer, sodium lignosulfonate as a reinforcing filler, and Fe^{3+} as a crosslinking agent. However, the resulting film exhibited limited ductility with an elongation at break of only 12%. Similarly, Guo *et al.*[15] incorporated multifunctional carbon dots into gelatin film systems. While this resulted in excellent antibacterial and antioxidant properties, the mechanical strength was compromised (6.4 MPa tensile strength). In another study, Cui *et al.*[16] employed carvacrol-loaded dialdehyde β-cyclodextrin to crosslink gelatin, blending it with carrageenan to moderately improve the strength of the film to 12 MPa. Critically, these approaches enhance either strength or single functionalities but fail to resolve the strength–toughness trade-off or achieve multifunctional integration. Therefore, establishing an effective method to balance strength and toughness without migratable glycerol while enabling functional integration in gelatin-based films is crucial.

Inspired by the hierarchical architecture of spider webs, where rigid radial threads (covalent networks) ensure structural integrity and flexible spiral threads (sacrificial hydrogen bonds) enable energy dissipation, an exceptional strength–toughness balance is achieved (Fig. 1a).[17–20] Therefore, we propose mimicking this hierarchy to enhance gelatin-based

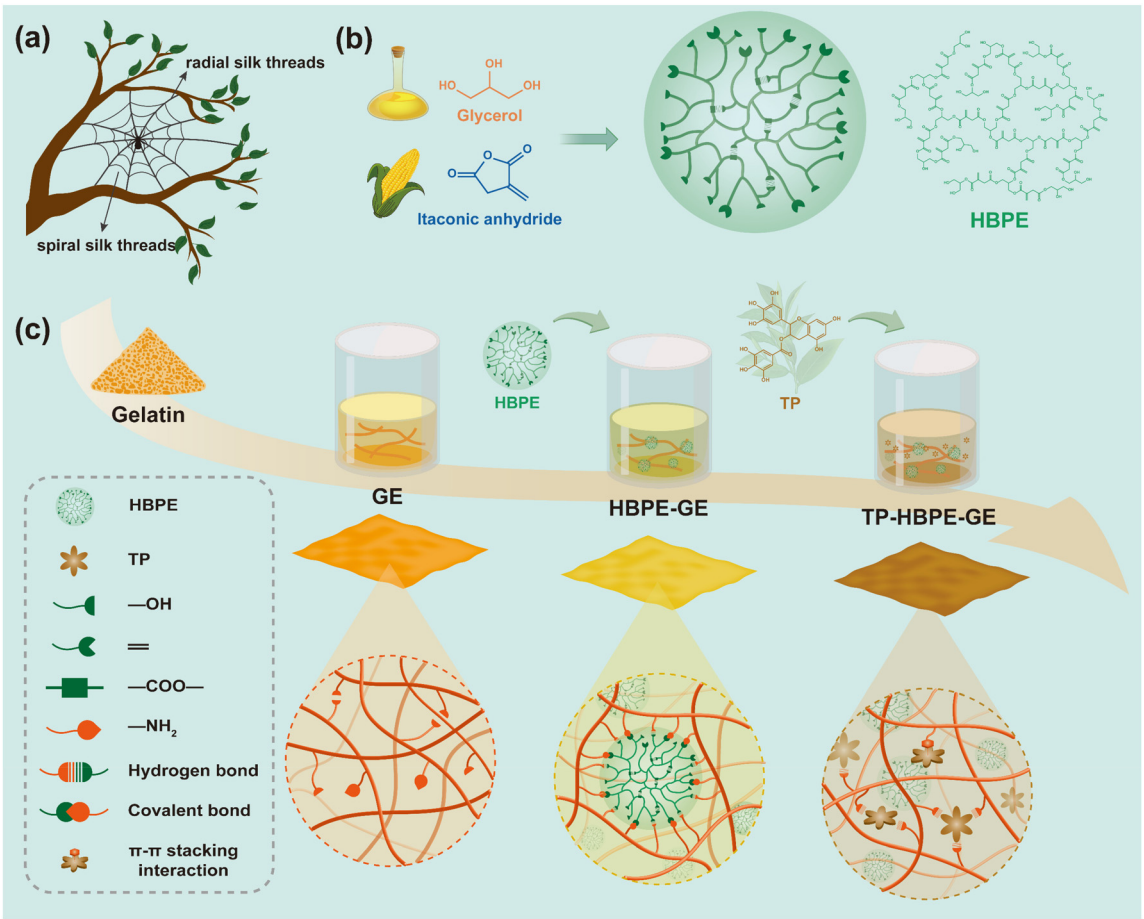

Fig. 1 (a) Structure of a spider's web. (b) Synthetic route of HBPE. (c) Preparation scheme for TP-HBPE-GE bioplastics.

films. Hyperbranched polymers (HBPs) are ideal candidates for constructing spider-web-like structures due to their dense branching architectures, abundant terminal groups, low chain entanglement, and high flexibility.[21] Their rich terminal functionalities enhance interactions with gelatin, while soft branches facilitate stress transfer and dissipation. This increases free volume and reduces intermolecular forces, synergistically improving strength and toughness.[22,23] However, to impart antibacterial and UV-resistant properties, tea polyphenols (TP), natural polyphenolic compounds with excellent ultraviolet (UV) shielding, antioxidant, and antibacterial activities,[24,25] are widely used in food and pharmaceutical applications. Their phenolic hydroxyl groups and aromatic structures can form supramolecular interactions with gelatin, potentially enhancing their mechanical properties, making TP an ideal functional modifier for gelatin-based films.[26]

We therefore propose a biomimetic dual-network strategy using HBPs and TP to modify gelatin without migratable glycerol. Considering compatibility and interfacial bonding, a specially designed bio-based hyperbranched polyester (HBPE) was synthesized from glycerol (a biodiesel by-product) and itaconic anhydride (glucose fermentation-derived), as shown in Fig. 1b. The terminal hydroxyl groups and vinyl crosslinking sites in HBPE enable the formation of a spider web-like structure *via* two pathways: (1) covalent "radial" networks, formed *via* the aza-Michael addition between GE amines and HBPE vinyl groups (analogous to the spider web's structural core), and (2) sacrificial "spiral" bonds, formed *via* supramolecular interactions (hydrogen bonding and π–π stacking) among TP, GE and HBPE, enabling energy dissipation (Fig. 1c). Concurrently, TP imparts UV shielding, antioxidant, and antimicrobial properties. Crucially, this strategy exemplifies advanced green chemistry: it utilizes renewable/waste-derived feedstocks (GE, glycerol), employs energy-efficient aqueous processing without harmful solvents, valorizes potential waste films into high-performance adhesives/coatings, and ensures biodegradability. By mimicking nature's design and intrinsically integrating functionality, we overcome the strength–toughness dichotomy in bioplastics while establishing a versatile and sustainable platform for high-performance gelatin-based films.

2. Methods

2.1 Materials

Gelatin (with a gum strength of approximately 100 g Bloom), itaconic anhydride (98%), and 1,1-diphenyl-2-picrylhydrazyl radical (DPPH) were purchased from Shanghai Macklin Biochemical Technology Co., Ltd. Glycerol was acquired from Tianjin Kermel Chemical Reagent Co., Ltd. Tea polyphenols (TP, 98%) were supplied by Shanghai Aladdin Biochemical Technology Co., Ltd. *Escherichia coli* (*E. coli*) and *Staphylococcus aureus* (*S. aureus*) strains were provided by the Shanghai Microbiological Culture Collection Center.

2.2 Synthesis of HBPE

Hyperbranched polyester (HBPE) was synthesized *via* melt polycondensation (Fig. 1b). Specifically, itaconic anhydride (IA, 11.5 g) and glycerol (GLY, 9.4 g) were charged into a 250 mL three-necked flask. After purging with nitrogen for 30 min to remove oxygen, the mixture was heated in an oil bath at 75 °C until it completely melted and homogenized. The temperature was then gradually elevated to 100 °C at 2 °C min^{-1} under continuous nitrogen protection. The polymerization proceeded with constant mechanical stirring at 550 rpm for 5 h, yielding a light-yellow, transparent, viscous liquid.

2.3 Preparation of gelatin-based bioplastic films

The film preparation is illustrated in Fig. 1c. First, 2.0 g of gelatin (GE) was dissolved in 18.0 g of deionized water with continuous stirring at 60 °C for 30 min to produce a homogeneous GE solution. Then, 0.7 g of HBPE was introduced into the GE solution, followed by reaction at 80 °C for 6 h. After cooling to 40 °C, 5 mL of TP solution with different mass fractions (0%, 1%, 3%, and 5%, w/w, relative to GE) was added dropwise under constant stirring at 40 °C for 1 h. Finally, the mixture was poured into a polytetrafluoroethylene mold and dried at room temperature (25 ± 2 °C) for 72 h to form the bioplastic films. The resulting films were labeled HBPE-GE, TP-HBPE-GE-1, TP-HBPE-GE-3, and TP-HBPE-GE-5 based on the TP content. For comparison, a control film (IAGL-GE) was prepared by mixing itaconic anhydride and glycerol (without polycondensation) into the GE solution, following the same procedure as that for HBPE-GE.

2.4 Characterization

2.4.1 Characterization of HBPE. Approximately 5.0 mg of HBPE was dissolved in DMSO-d_6 and subjected to nuclear magnetic resonance (NMR) analysis using a 600 MHz spectrometer to acquire the ^{1}H NMR and ^{13}C NMR spectra. HBPE was then dissolved in deionized water to prepare an aqueous solution with a concentration of 5 mg mL^{-1}. The molecular weight of HBPE was determined using gel permeation chromatography (GPC) with a differential refractive index (DRI) detector and two PL aquagel-OH MIXED-M columns (8 μm, 7.5 mm × 300 mm). Measurements were conducted with an injection volume of 100 μL and ultrapure water as the mobile phase at a flow rate of 1 mL min^{-1}.

2.4.2 Characterization of the TP-HBPE-GE bioplastic films. The bioplastic films (2 × 2 cm^2) were analyzed using a Bruker Fourier-transform infrared (FTIR) spectrometer in attenuated total reflectance (ATR) mode. Spectra were recorded from 4000 to 400 cm^{-1} with 32 scans at a resolution of 2 cm^{-1}. X-ray diffraction (XRD) patterns were acquired using a diffractometer (40 kV, 30 mA) over a 2θ range of 5°–60° at 5° min^{-1}. The surface elemental composition and chemical states were characterized using X-ray photoelectron spectroscopy (XPS; Thermo Scientific ESCALAB Xi+) with a monochromatic Al Kα source (1486.68 eV), operated at 15 kV and 10 mA.

Light transmittance (200–800 nm) was measured using a Cary 5000 UV–Vis spectrophotometer. The color parameters (L^*, a^*, b^*, and ΔE^*) were determined using an X-Rite Ci7800 spectrophotometer against a white background (L^* = 95.86, a^* = −0.36, and b^* = 2.1). The whiteness (WI) and yellowness (YI) indices were calculated from five measurements per sample using eqn (2-1) and (2-2), respectively.

$$\mathrm{WI} = 100 - \sqrt{(100 - L^*)^2 + a^{*2} + b^{*2}} \quad (2-1)$$

$$\mathrm{YI} = \frac{142.86 \times b^*}{L^*} \quad (2-2)$$

The bioplastic samples were conditioned at 25 ± 2 °C and a relative humidity (RH) of 58 ± 3% for 48 h, after which the samples were cut into dumbbell-shaped specimens. The thickness was averaged from three positions using a digital gauge. Tensile tests were performed on an AI-7000-NGD universal testing machine (10 mm min^{-1}, 20 mm grip distance). Toughness was derived from stress–strain curves, with five replicates per group.

The surface and cross-sectional morphologies of the fractured bioplastic samples were sputter-coated with a 5 nm layer of platinum and imaged using FESEM (Hitachi SU4800, 5 kV, 8 mm working distance). Surface roughness, including the average roughness (R_a) and the maximum height (R_z), was quantified using laser confocal microscopy (ISO 4287), with three measurements taken for each sample.

Thermogravimetric analysis (TGA Q500) of the bioplastic films was performed under nitrogen from 40 to 600 °C at 10 °C min^{-1}. Glass transition temperatures (T_g) of the bioplastic films were determined using a DSC-Q2000 with a temperature scan from −70 to 110 °C at 10 °C min^{-1} under nitrogen.

The water vapor transmission rate (WVT) of the bioplastic films with a diameter of 70 mm was determined at 38 °C and 75% relative humidity using a C360H tester. Water contact angles (WCA) were determined using a Dataphysics OCA 40 micro goniometer, with 5.0 ± 0.1 μL of deionized water dispensed onto the film surface at 5 μL s^{-1}. Static angles were averaged from five measurements.

The DPPH (2,2-diphenyl-1-picrylhydrazyl) radical scavenging assay was used to evaluate the antioxidant activity. Bioplastic film samples (20 mg) were immersed in 4 mL of 0.1 mM DPPH (prepared in a 1 : 1 v/v ethanol–water solution) and incubated in the dark for 60 min. The absorbance was then measured at 517 nm using a UV-Vis spectrophotometer. A DPPH solution without the sample served as the control. The radical scavenging activity (%) was calculated as

$$\text{DPPH radical scavenging activity}\,(\%) = \frac{A_c - A_S}{A_S} \quad (2-3)$$

where A_c is the absorbance of the DPPH solution without the sample (the control) and A_s is the absorbance of the bioplastic film.

The antibacterial performance against *S. aureus* (Gram-positive) and *E. coli* (Gram-negative) was tested using the ISO 22196:2011 colony counting method. The culture media and phosphate-buffered saline (PBS) were prepared in accordance with the Chinese national standard GB/T 21866-2008. The bacterial suspension (10 μL) was spread onto the bioplastic samples, incubated at 37 °C and 90% relative humidity for 2 h, then transferred to 10 mL of PBS and vortexed to detach the bacteria. Serial dilutions of these suspensions were plated onto solid culture media and incubated at 37 °C for 24 h. The antibacterial rate (%) was calculated as

$$\text{Antibacterial rate}\,(\%) = \frac{N_0 - N_1}{N_0} \times 100\% \quad (2-4)$$

where N_0 is the colony count of the control and N_1 is the colony count of the bioplastic sample.

The freshly prepared bioplastic films were conditioned (25 ± 2 °C, 50 ± 5% RH) for 48 h before testing. Cherry tomatoes with uniform ripeness and no visible defects were randomly divided into three groups: unwrapped (the control group), wrapped in commercial PVC film, and wrapped in TP-HBPE-GE bioplastic film. All samples were stored at 25 ± 2 °C for 15 days. Weight loss and firmness were measured at 0, 3, 6, 9, 12, and 15 days to evaluate preservation performance. Cherry tomato hardness was determined using a universal testing machine equipped with a compression fixture. Samples were compressed vertically until reaching one-third of their original height, and the peak force recorded at this deformation point was defined as the hardness index. Weight loss was calculated as

$$\text{Weight loss}\,(\%) = \frac{m_1 - m_0}{m_0} \times 100\% \quad (2-5)$$

where m_0 is the initial weight of the cherry tomato, and m_1 is its weight after storage.

The recyclability of the bioplastic samples was tested using three different methods: water wetting, steam treatment, and thermal activation. The pretreated samples were reshaped and air-dried to assess their moldability. Packaging bags were fabricated *via* heat sealing using either a commercial sealing machine or wet adhesion to examine processability. The self-healing properties were studied by creating surface scratches on the bioplastics and repairing them using three methods: water-induced healing, steam-induced healing, and heat-press-assisted healing. The changes in surface morphology before and after repair were observed using a HIROX KH-8700 3D digital microscope. The recyclability of discarded bioplastic fragments was evaluated through thermal pressing or solution casting.

Soil burial tests (ISO 14855-1:2012) were conducted under controlled conditions. At predefined degradation intervals (0.5, 1, 1.5, 2, 2.5, 3, 3.5, and 4 weeks), the samples were cleaned and weighed to determine the residual mass. Biodegradation rates were calculated as follows:

$$\text{Biodegradation rate}\,(\%) = \frac{m_2 - m_1}{m_1} \times 100\% \quad (2-6)$$

where m_1 is the initial mass of the bioplastic sample and m_2 is the residual mass after degradation for a given period.

3. Results and discussion

3.1 Structural analysis of HBPE

The structural characteristics of HBPE were systematically characterized using ^{1}H NMR, ^{13}C NMR, and GPC. As shown in Fig. S1a, the distinct proton signals at 4.4 and 4.7 ppm were attributed to the hydroxyl groups of glycerol. Following the reaction with itaconic anhydride, these signals shifted to 3.85 ppm with significantly reduced intensity. Meanwhile, a new methylene peak appeared at 4.04 ppm, adjacent to that of the ester group, indicating that glycerol and itaconic anhydride underwent polycondensation to form HBPE. The branched (D), linear (L), and terminal (T) units of HBPE were analyzed *via* ^{13}C NMR (Fig. S1b), and the degree of branching was calculated to be 0.53, indicating a highly branched molecular architecture. GPC analysis (Fig. S2) revealed that the number-average molecular weight (M_n) of HBPE was 7514 Da, the weight-average molecular weight (M_w) was 10 200 Da, and the polydispersity index was 1.36. These results demonstrate that HBPE synthesized from glycerol and itaconic anhydride possesses a highly branched topological structure resembling a spider's web.

3.2 Structural characterization of the gelatin-based bioplastic films

The chemical structure of gelatin-based films was investigated using FT-IR spectroscopy. As shown in Fig. 2a, all gelatin-based films exhibited typical characteristic absorption bands corresponding to the amide A, B, I, II, and III regions.[27] Notably, IAGL-GE and HBPE-GE films showed red-shifts in their characteristic bands compared to the pure gelatin film. The amide A band shifted from 3305 cm^{-1} to 3291 cm^{-1}, the amide B band shifted from 2973 cm^{-1} to 2930 cm^{-1}, and the amide II and III bands exhibited minor shifts (from 1541 to 1538 cm^{-1} and from 1236 to 1231 cm^{-1}, respectively). These shifts are attributed to the Aza-Michael addition reaction occurring between the vinyl double bonds of IA/HBPE and the amino groups of gelatin (Scheme S1), which reduced the content of free amino groups and altered the electron density distribution in peptide bonds.[28] Upon incorporation of TP, the TP-HBPE-GE film displayed further shifts in the amide II and III bands, which shifted to 1535 cm^{-1} and 1229 cm^{-1}, respectively. This phenomenon is associated with extensive hydrogen bonding between the phenolic hydroxyl groups of TP and the –CONH– or –OH groups in gelatin, which partially restricts the vibrational freedom of the peptide backbone. These results are consistent with the red-shifts induced by hydrogen bonds observed between phenolic compounds and gelatin, as reported by Liu *et al.*[29]

XPS analysis was performed on GE, IAGL-GE, and HBPE-GE films to investigate the covalent crosslinking reaction between

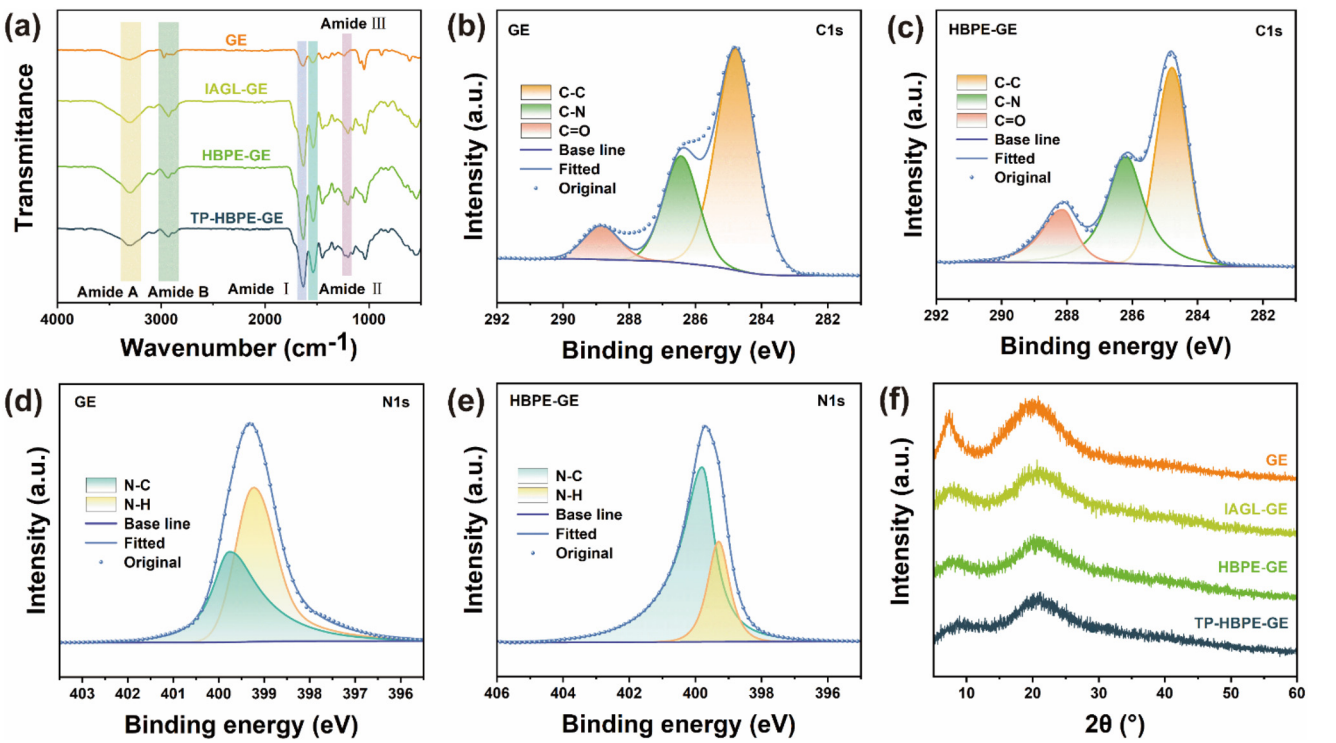

Fig. 2 (a) FT-IR spectra of GE, IAGL-GE, HBPE-GE, and TP-HBPE-GE bioplastic films. (b and c) High-resolution XPS spectra of C 1s and (d and e) N 1s of GE and HBPE-GE bioplastic films. (f) XRD patterns of GE, IAGL-GE, HBPE-GE, and TP-HBPE-GE bioplastic films.

gelatin and HBPE. As shown in Fig. 2b and c and Fig. S3a, all gelatin-based films displayed three distinct peaks in their C 1s spectra at 284.6 eV (C–C), 285.8 eV (C–N), and 287.7 eV (C═O). This is consistent with previous reports on the structure of gelatin.[30] The proportion of C–N bonds increased significantly, rising from 26% in the pure GE film to 40% in the IAGL-GE film and 36% in the HBPE-GE film. This indicates the formation of new C–N covalent linkages through the Aza-Michael addition between the amino groups in gelatin and the vinyl double bonds present in IA and HBPE. Complementary evidence was obtained from high-resolution N 1s spectra (Fig. 2d, e and Fig. S3b). All samples presented two characteristic peaks at 399.5 eV (N–H) and 400.2 eV (N–C). The proportion of N–H bonds decreased from 56.5% in the pure GE film to 23.6% and 29.1% in the IAGL-GE and HBPE-GE films, respectively, while the proportion of N–C bonds increased from 43.5% in the pure GE film to 76.4% in the IAGL-GE film and 70.9% in the HBPE-GE film. This directly correlates with the consumption of free amino groups in gelatin during covalent crosslinking. It confirms that gelatin participates in the Aza-Michael reaction with HBPE, resulting in the conversion of N–H bonds to N–C bonds. Overall, the combined FT-IR and XPS results provide evidence for the formation of covalent crosslinking between HBPE and gelatin *via* the Aza-Michael addition reaction, as well as extensive hydrogen bonding between HBPE, TP, and gelatin.

The crystalline structure of gelatin-based films modified with HBPE and TP was investigated using XRD analysis. As shown in Fig. 2f, the pure GE film exhibited two characteristic diffraction peaks at $2\theta \approx 7°$ and 20°, corresponding to the crystalline domains of collagen-like triple helices and the amorphous single-chain phase in gelatin, respectively.[31] Following covalent crosslinking of IA or HBPE with the amino groups of gelatin, the peak intensity at $2\theta \approx 7°$ notably reduced, indicating that the crosslinked network hindered ordered molecular chain alignment and suppressed reconstruction of triple-helix-like structures.[32] After introducing TP, the peak intensity at $2\theta \approx 7°$ decreased further. This is due to the phenolic hydroxyl groups in TP forming extensive hydrogen-bond interactions with –CONH– or –OH groups in gelatin, thereby interfering with the native chain alignment of gelatin.[33] These results align with the FT-IR and XRS data, confirming that HBPE and TP facilitated covalent cross-linking and hydrogen bond networks, reducing the crystallinity of gelatin-based films.

3.3 Basic properties and microscopic morphology of gelatin-based bioplastic films

Mechanical performance is crucial in determining their practical applications, as it affects durability and reliability. Pure gelatin film is extremely brittle due to the inherent rigidity of molecular chains and strong intermolecular interactions, severely limiting its applications.[34] However, the mechanical properties of gelatin-based films can be effectively modulated by introducing HBPE with a unique, spider-web-inspired architecture (Fig. 3a). With 25% HBPE loading, the HBPE-GE25 film exhibited a tensile strength of 33.8 MPa and an elongation at break of 21.6%. Interestingly, when the HBPE content increased to 45%, the tensile strength decreased to 11.0 MPa, but ductility enhanced with an elongation at break of 125.3%. The toughness of the HBPE-GE film increased as the HBPE content increased from 25% to 45% (Fig. 3b). This was mainly due to the highly branched structure of HBPE, which acts as a crosslinker to react with gelatin, constructing a crosslinking network that resembles the radial structure of a spider's web and can withstand stress. Meanwhile, HBPE and gelatin formed an extensive hydrogen bond network that can dissipate stress effectively, resembling the spiral structure of a spider's web. These dual network interactions simultaneously enhanced the tensile strength and toughness of the HBPE-GE film, enabling adjustable mechanical properties. The tunability of the mechanical properties was visually demonstrated through loading tests (Fig. 3c). The HBPE-GE 25 film withstood a 1 kg load without fracturing, while the HBPE-GE 45 film exhibited excellent flexibility and could endure complex deformations, including bending and knotting. For optimal strength–toughness balance, the HBPE-GE 35 film was identified as an ideal candidate for further investigation and is denoted as HBPE-GE.

For comparison, the control film (IAGL-GE) prepared by replacing hyperbranched HBPE with unpolymerized itaconic anhydride and glycerol exhibited inferior mechanical properties, with the tensile strength and elongation at break measured at 7.6 MPa and 39.3%, respectively. In contrast, the HBPE-GE film demonstrated significantly enhanced performance, with a tensile strength and an elongation at break of 17.5 MPa and 55.9%, respectively (Fig. 3d, e and Fig. S4). This confirms that HBPE's branched architecture critically improves both strength and toughness simultaneously. Further incorporation of TP increased the tensile strength from 17.5 MPa to 25.1 MPa, while reducing the elongation at break from 55.9% to 44.6%. This occurs because TP forms multiple hydrogen bonds with both HBPE and gelatin, thereby reinforcing the sacrificial bond network. Additionally, TP engages in π–π stacking interactions with aromatic moieties in gelatin (Fig. 3g).[35] These combined effects strengthen intermolecular binding and create a denser three-dimensional network, ultimately improving tensile strength. Although chain mobility is partially restricted, the TP-HBPE-GE-5 film retained favorable toughness while exhibiting a tensile strength significantly exceeding that of most reported gelatin-based films and comparable to, or even surpassing, that of certain petroleum-based and biodegradable plastics (Fig. 3f and Table S1). This unique integration of high strength and ductility, overcoming the conventional strength–ductility trade-off in bioplastics, establishes it as a viable alternative to conventional packaging films for sustainable applications.

The appearance of the TP-HBPE-GE-5 film is shown in Fig. 3a. All films exhibited high optical transparency (Fig. S5a). Fig. S5b and S5c present the chromatic characteristics of the gelatin-based films, including color difference (ΔE^*), whiteness index (WI), and yellowness index (YI). While the IAGL-GE and HBPE-GE films showed negligible changes in color para-

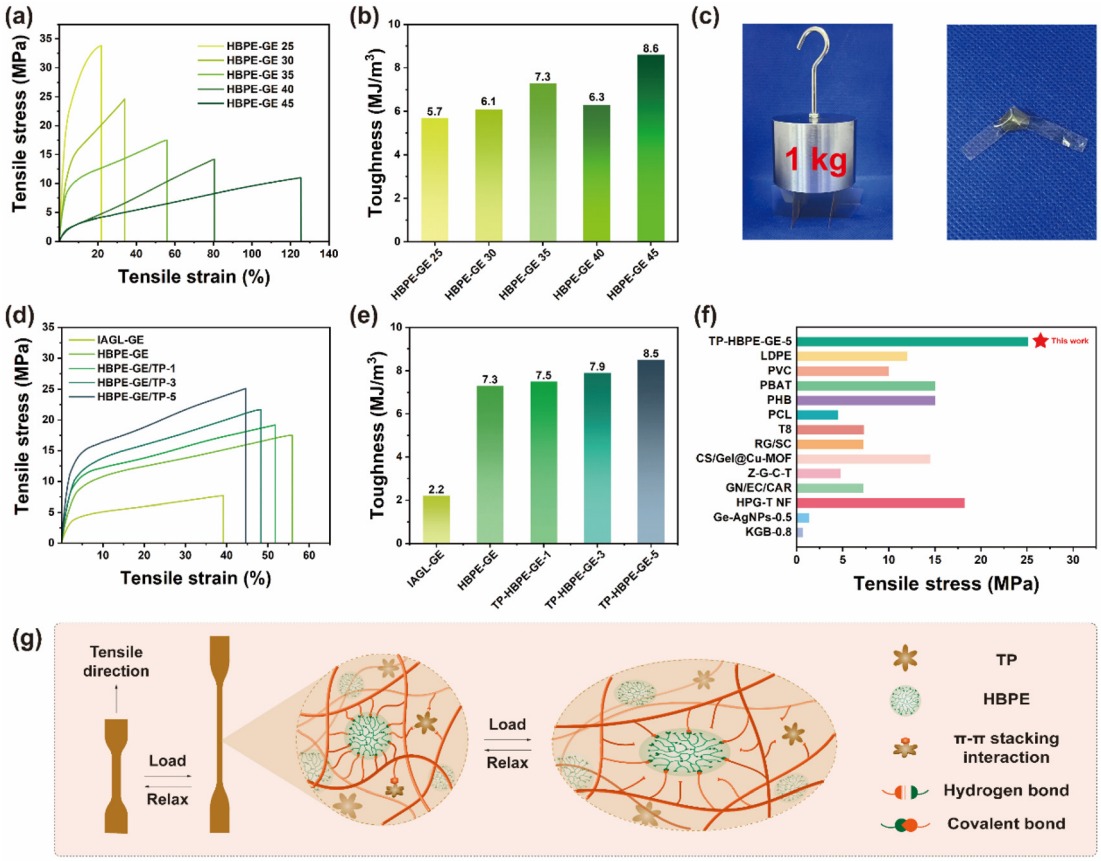

Fig. 3 Mechanical properties and structural characterization of TP-HBPE-GE films. (a) Stress–strain curves, (b) toughness, and (c) photo of the loading test. (d) Stress–strain curves and (e) toughness of IAGL-GE, HBPE-GE, TP-HBPE-GE-1, TP-HBPE-GE-3, and TP-HBPE-GE-5 films. (f) Mechanical strength comparison of the TP-HBPE-GE-5 film with petroleum-based plastics, biodegradable plastics, and other gelatin-based films. (g) Schematic illustration of the molecular interactions in TP-HBPE-GE films.

meters, the incorporation of TP significantly altered the optical properties. As the TP content increased from 0% to 5%, lightness (L^*) decreased from 88.9 to 57.6, accompanied by a corresponding increase in ΔE^* from 17.7 to 59.3. This significant color variation in TP-HBPE-GE films can be attributed to TP's distinctive molecular architecture, which induces both light absorption and scattering phenomena.[36]

To further evaluate the influence of TP on the optical transmittance of gelatin-based films, a UV-vis spectrophotometer was used to perform full-wavelength (200–800 nm) scanning (Fig. S6a). The results (Fig. S6b) demonstrate that visible light transmittance decreased from 76.8% to 48.2% with increasing TP loading. Crucially, even at the highest TP content (TP-HBPE-GE-5), the film maintained sufficient optical clarity for practical use, evidenced by clear visibility of background patterns and text (Fig. 4a). This indicates that the films meet the visibility requirements essential for food packaging applications despite the reduction in transmittance. In the UV region (200–400 nm), TP demonstrated significant UV-blocking capabilities. As the TP content increased from 0% to 5%, the UV-blocking efficiency of the films improved from 87.2% to 99.8% (Fig. S6c). This improvement originated from the synergistic effect of TP's conjugated π-electron systems and phenolic hydroxyl groups, which enable broad-spectrum UV absorption through electronic transitions.[37,38] To visually validate the UV-shielding performance, photochromic testing was conducted using UV-responsive indicator cards covered with different films and exposed to UV irradiation (Fig. 4b). Under UV irradiation, a distinct purple color appeared in areas covered by the IAGL-GE and HBPE-GE films, whereas the region covered by the TP-HBPE-GE-5 film exhibited negligible chromatic change. This macroscopic observation confirmed that adding TP significantly enhanced the UV-shielding efficiency of gelatin-based films. This is consistent with the UV-vis transmittance spectrum results (Fig. S6a), demonstrating the potential of these films as UV-shielding packaging materials.

The fracture morphologies of gelatin-based films under stress were characterized using SEM (Fig. 4c). All films exhibited ductile fracture characteristics with distinct propagation patterns. IAGL-GE films showed cracks propagating linearly along the fracture surface, resulting in a relatively smooth fracture plane. In contrast, HBPE-GE films displayed significantly increased surface roughness and more tortuous paths featuring deflections and branching. This can be attributed to the

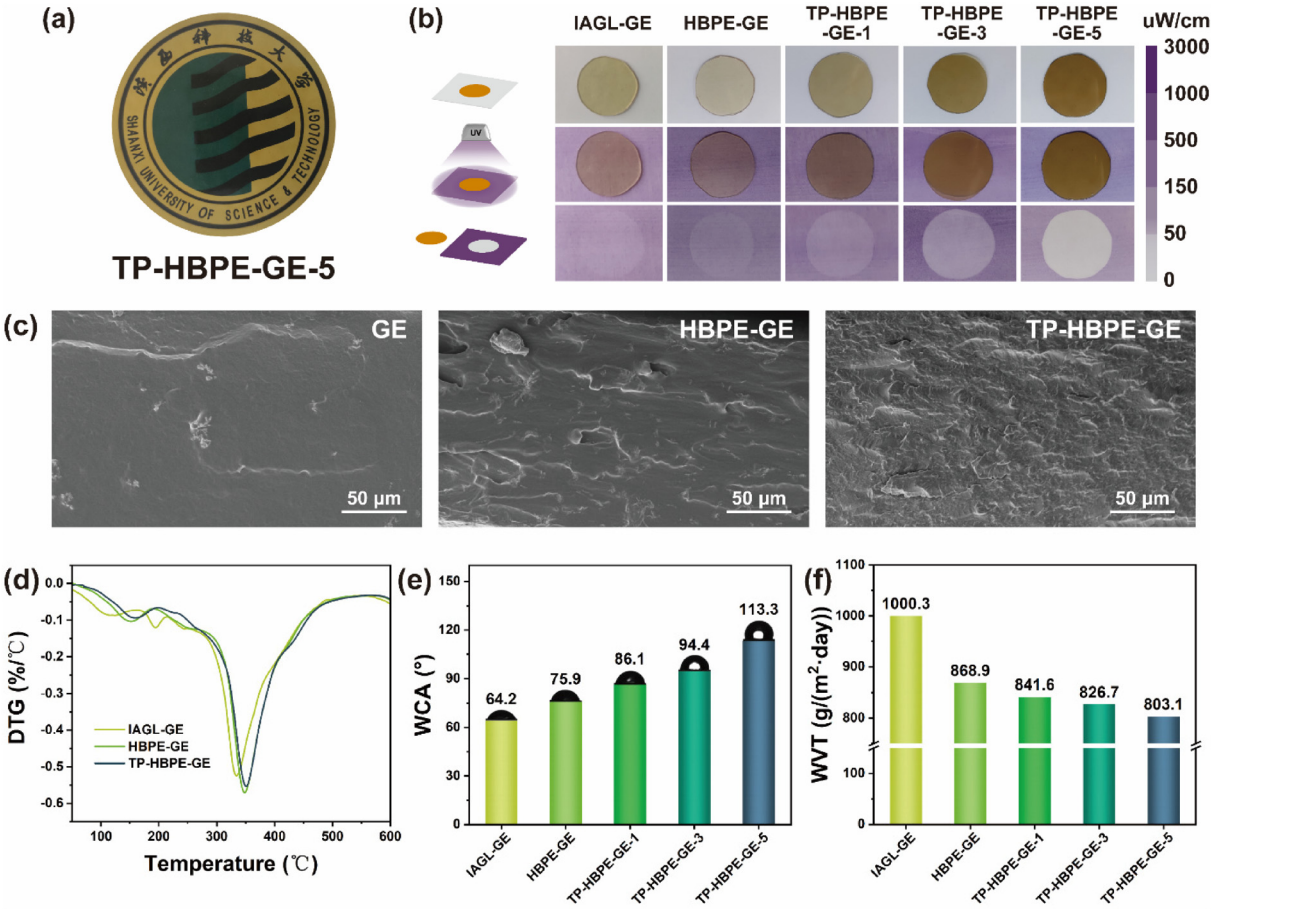

Fig. 4 (a) Optical images of TP-HBPE-GE-5. (b) Images of UV indicator cards before and after UV exposure for the following films: IAGL-GE, HBPE-GE, TP-HBPE-GE-1, TP-HBPE-GE-3, and TP-HBPE-GE-5. (c) SEM images of IAGL-GE, HBPE-GE, and TP-HBPE-GE-5 films. (d) DTG curves of IAGL-GE, HBPE-GE, and TP-HBPE-GE films. (e) Water contact angles (WCA) and (f) water vapor transmission rates (WVT) of IAGL-GE, HBPE-GE, TP-HBPE-GE-1, TP-HBPE-GE-3, and TP-HBPE-GE-5 films.

highly branched topological structure of HBPE, which enables multidirectional stress redistribution. The distortion of the resulting crack path demonstrates the critical role of HBPE in improving the toughness of gelatin-based films, which is consistent with previous mechanical analyses.[39] The incorporation of TP resulted in a rougher fracture surface in the TP-HBPE-GE film. This indicates that TP molecules form synergistic supramolecular interactions with both gelatin and HBPE *via* π–π stacking and hydrogen bonds. These non-covalent interactions create energy-dissipation domains that fail preferentially under stress, thereby hindering the propagation of macrocracks.[40] The combination of covalent crosslinking between HBPE and gelatin and supramolecular interactions (π–π stacking and hydrogen bonds) between HBPE, TP, and gelatin collectively altered the fracture behavior of the TP-HBPE-GE film. The resulting crack propagation pattern was consistent with the improvements observed in mechanical performance.

To evaluate the interfacial compatibility of the TP-HBPE-GE film, its three-dimensional surface morphology was analyzed using laser scanning confocal microscopy (LSCM). As illustrated in Fig. S7a, the respective peak-to-valley distances for IAGL-GE, HBPE-GE, and TP-HBPE-GE were found to be 37.2 μm, 35.0 μm, and 44.3 μm, respectively. This indicates homogeneous distribution of IA, HBPE, and TP within the gelatin matrix, with no detectable macrophase separation. Quantitative roughness analysis further validated this compatibility (Fig. S7b). No statistically significant differences were observed in the arithmetic average roughness (R_a) and ten-point average roughness (R_z) values of IAGL-GE, HBPE-GE, and TP-HBPE-GE films, with global averages of 2.2 μm (R_a) and 0.6 μm (R_z) across five replicates. These results demonstrate good compatibility between the components within the gelatin-based film.

The thermogravimetric profiles of IAGL-GE, HBPE-GE, and TP-HBPE-GE films (Fig. S8 and Fig. 4d) exhibited two dominant thermal degradation stages. The first stage (50–150 °C) corresponded to moisture evaporation, while the second stage (300–400 °C) reflected the decomposition of the collagen-like triple-helical structure and crosslinked network of gelatin.[41] Notably, the IAGL-GE film exhibited accelerated mass loss at 100–250 °C, primarily attributed to glycerol decomposition.[42] The temperatures at which 5% weight loss occurred increased

progressively from 133.9 °C (IAGL-GE) to 155.1 °C (HBPE-GE) and 167.2 °C (TP-HBPE-GE), indicating that the addition of HBPE and TP improved the initial thermal resistance. The maximum decomposition temperatures followed a similar trend (333.5 °C, 347.7 °C, and 350.5 °C), highlighting the stabilizing effect during main-chain degradation. Furthermore, residual char yields increased from 26.2% (IAGL-GE) to 30.1% (TP-HBPE-GE), reflecting the enhanced carbonization capacity of the TP-HBPE-GE film. This is due to covalent crosslinking between HBPE and gelatin, as well as the relatively high aromatic content of the system.[43] DSC analysis (Fig. S9) revealed the following T_g values: 30.8 °C for IAGL-GE, 40.5 °C for HBPE-GE, and 53.3 °C for TP-HBPE-GE. The relatively low T_g of IAGL-GE was due to the plasticizing effect of glycerol through free-volume expansion. Upon the incorporation of HBPE, the T_g of the HBPE-GE film increased to 40.5 °C. This increase in T_g can be attributed to the covalent crosslinking network and hydrogen bond interactions that restrict chain mobility,[44] while the introduction of TP increased the T_g further to 53.3 °C in the TP-HBPE-GE film. This was mainly ascribed to synergistic effects, including the formation of supramolecular hydrogen bonds and π–π stacking within the system, as well as the aromatic rigidity imparted by the TP component.[45]

The hydrophobicity of the TP-HBPE-GE film surfaces was characterized using static water contact angle measurements. As shown in Fig. 4e, the IAGL-GE film exhibited a WCA of 64.2°, reflecting the intrinsic hydrophilicity of the polar groups in gelatin and plasticizers (itaconic anhydride and glycerol). In contrast, the WCA of the HBPE-GE film increased to 75.9°. This is due to covalent crosslinking between HBPE and gelatin, which reduces the number of hydrophilic groups and forms a dense, three-dimensional network that acts as a physical moisture barrier. Interestingly, the surface hydrophobicity of the TP-HBPE-GE film increased with the introduction of TP. As TP increased from 0% to 5%, the WCA increased from 75.9° to 113.3°. This is primarily due to the aromatic rings of TP migrating to the film–air interface, where π–π stacking creates low-surface-energy domains,[46] effectively converting the hydrophilic surface to hydrophobic. WVT is a key indicator used to assess the barrier properties of food packaging films. As shown in Fig. 4f, the WVT of the IAGL-GE film was 1000.3 g $(m^2\ day)^{-1}$, which is attributed to the strong hydrophilicity of gelatin, itaconic anhydride and glycerol. Following covalent crosslinking between HBPE and GE, the WVT of the HBPE-GE film decreased by 13%, from 1000.3 to 868.9 g $(m^2\ day)^{-1}$, due to structural densification. The incorporation of TP from 0% to 5% resulted in a further decrease in the WVT of the TP-HBPE-GE film, from 868.9 to 803.1 g $(m^2\ day)^{-1}$, achieving a total reduction of 18%. This is mainly due to the combined effects of HBPE and TP forming a compact network structure *via* covalent crosslinking and supramolecular hydrogen bond and π–π stacking interactions. Additionally, the enhanced surface hydrophobicity effectively inhibits water molecule adsorption and permeation, thereby improving the barrier properties of TP-HBPE-GE films.[47]

3.4 Application performance of gelatin-based bioplastics in food preservation

The antioxidant functionality of food packaging films is essential for mitigating oxidative spoilage and preserving nutritional quality. The DPPH radical scavenging assay revealed limited antioxidant activity in IAGL-GE and HBPE-GE films (38.0% at 4 mg mL^{-1}), as evidenced by a slight color change of the DPPH solution from purple to light purple. These results were comparable to those of the control group (Fig. 5a and Fig. S10). This was attributed to the weak π-electron delocalization capacity of phenylalanine residues in gelatin.[48] However, incorporating TP significantly enhanced the antioxidant performance. As the TP content increased from 0% to 5%, the DPPH scavenging rate increased dramatically from 38.0% to 88.6%. This was attributed to the abundant phenolic hydroxyl groups in TP acting as hydrogen donors to quench free radicals.[49]

The antibacterial activity of the TP-HBPE-GE films was evaluated by determining their inhibition rate against *E. coli* and *S. aureus* using the colony counting method. As shown in Fig. 5b, the introduction of TP led to a significant reduction in bacterial colonies within the TP-HBPE-GE films, indicating a pronounced enhancement in antibacterial efficacy. Complete bacterial eradication was achieved at a TP loading of 5% (survival rate: 0%), whereas TP-HBPE-GE-1 exhibited survival rates of 15.4% (*E. coli*) and 13.5% (*S. aureus*) (Fig. S11). The potent bactericidal effect of TP-HBPE-GE-5 is attributed to the polyphenolic hydroxyl groups in TP disrupting bacterial membrane integrity, inducing cytoplasmic leakage and subsequently causing cell death.[50]

The freshness preservation efficacy for unpacked, PVC-packed, and TP-HBPE-GE-5 film-packed cherry tomatoes was evaluated (Fig. 5a and Fig. S12). By day 9, unpacked tomatoes suffered severe signs of dehydration, while those in PVC packaging had visible mould, followed by progressive surface spoilage by day 12. Remarkably, tomatoes packed in TP-HBPE-GE-5 films maintained optimal visual quality throughout a 15-day storage period, with no detectable microbial growth or physiological deterioration, demonstrating the superior preservation performance of TP-HBPE-GE-5 packaging films. As shown in Fig. 5d and e, unpacked tomatoes deteriorated rapidly during storage, with firmness decreasing from 13.6 N to 1.4 N and weight loss reaching 35.1%. This decline was due to the tomatoes being directly exposed to ambient air, which promoted water evaporation, tissue dehydration, and microbial invasion. PVC-packaged tomatoes showed marginally improved performance, with firmness decreasing from 11.5 N to 4.2 N and weight loss limited to 7.5%. However, the high moisture resistance of PVC leads to humidity building up inside the PVC package, contributing to an increase in anaerobic respiration by-products and mould growth. This compromises the structural integrity of the fruit. In contrast, the TP-HBPE-GE-5 film demonstrated superior preservation efficacy, with tomato firmness declining moderately from 12.7 N to 8.3 N and weight loss restricted to 5.5%. This was attributed to the dense hydrogen-bond network of the TP-HBPE-GE-5 film, which allowed

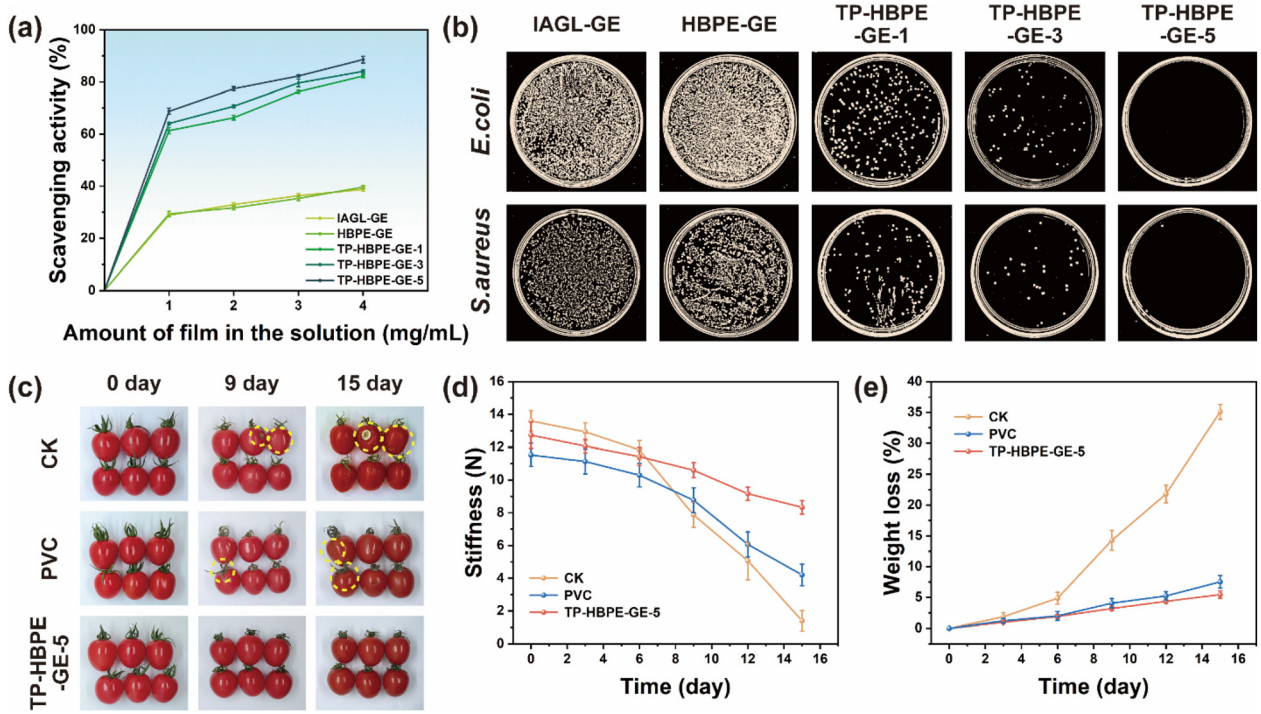

Fig. 5 (a) Corresponding scavenging activities of IAGL-GE, HBPE-GE, TP-HBPE-GE-1, TP-HBPE-GE-3, and TP-HBPE-GE-5 films. (b) Representative colony images of *E. coli* and *S. aureus* after treatment with the IAGL-GE, HBPE-GE, TP-HBPE-GE-1, TP-HBPE-GE-3, and TP-HBPE-GE-5 films. (c) Optical images, (d) hardness, and (e) weight loss rate of unpacked, PVC-packed, and TP-HBPE-GE-5 film-packed cherry tomatoes at different storage times.

controllable water vapor permeability and maintained optimal humidity inside the package. Furthermore, the antioxidant and antibacterial properties of the TP-HBPE-GE-5 film effectively suppressed microbial growth and oxidative decay. In summary, the TP-HBPE-GE-5 film was more effective at preserving cherry tomatoes than conventional PVC packaging films. This was due to the combined effects of the regulation of moisture permeability mediated by the hydrogen bond network structure, and antibacterial and antioxidant properties. These properties make the TP-HBPE-GE-5 film a highly promising option for preserving perishable fruits and vegetables.

3.5 The sustainability of gelatin-based bioplastic films

The sustainability of gelatin-based films throughout their lifecycle is crucial for expanding future applications. Fig. 6 presents a comprehensive evaluation of TP-HBPE-GE films, focusing on processability, self-healing ability, recyclability, and biodegradability to demonstrate their potential for environmentally friendly applications. The processability of the TP-HBPE-GE films was evaluated using three treatment methods: water wetting, steam treatment, and thermal activation at 80 °C (Fig. 6a). These methods effectively disrupted the intermolecular hydrogen bond network within the films, enabling molecular chain reorganization and the formation of complex shapes (*e.g.*, zigzag, spiral, and curved geometries) by reforming the hydrogen bond network *via* water or thermal activation. This demonstrates excellent plasticity of the film. To further investigate the processing applicability of the TP-HBPE-GE films, sealed bags were prepared using two methods: heat sealing and water-assisted bonding. As shown in Fig. 6b, sealed bags can be obtained by either directly heat sealing two pieces of the TP-HBPE-GE film using a commercial heat sealer or by self-bonding two pieces of the film after immersing them in water for 5 min. The resulting TP-HBPE-GE sealed bags can encapsulate oils (*e.g.*, soybean oil) and powders. This indicates that the TP-HBPE-GE films are suitable for diverse packaging applications. The excellent processability of the TP-HBPE-GE films is attributed to reversible hydrogen bond dissociation and reformation in response to stimuli. As illustrated in Fig. 6c, the hydrogen bond network between gelatin, HBPE and TP dissociates upon water or heat treatment, while the hydrogen bonds reform during the drying or cooling process to achieve molecular rearrangement.[51] Thus, the TP-HBPE-GE films can be processed in a controlled manner under water or thermal stimuli by breaking and reorganizing hydrogen bonds.

In practice, bioplastic films inevitably sustain mechanical damage, resulting in a shorter service life. To address this issue, we evaluated the intrinsic self-healing ability of TP-HBPE-GE-5 films using three distinct restoration strategies. As shown in Fig. 7a, controlled surface scratches (with a width of approximately 35–52 μm) were manually created with a blade to simulate mechanical damage. The TP-HBPE-GE-5 film

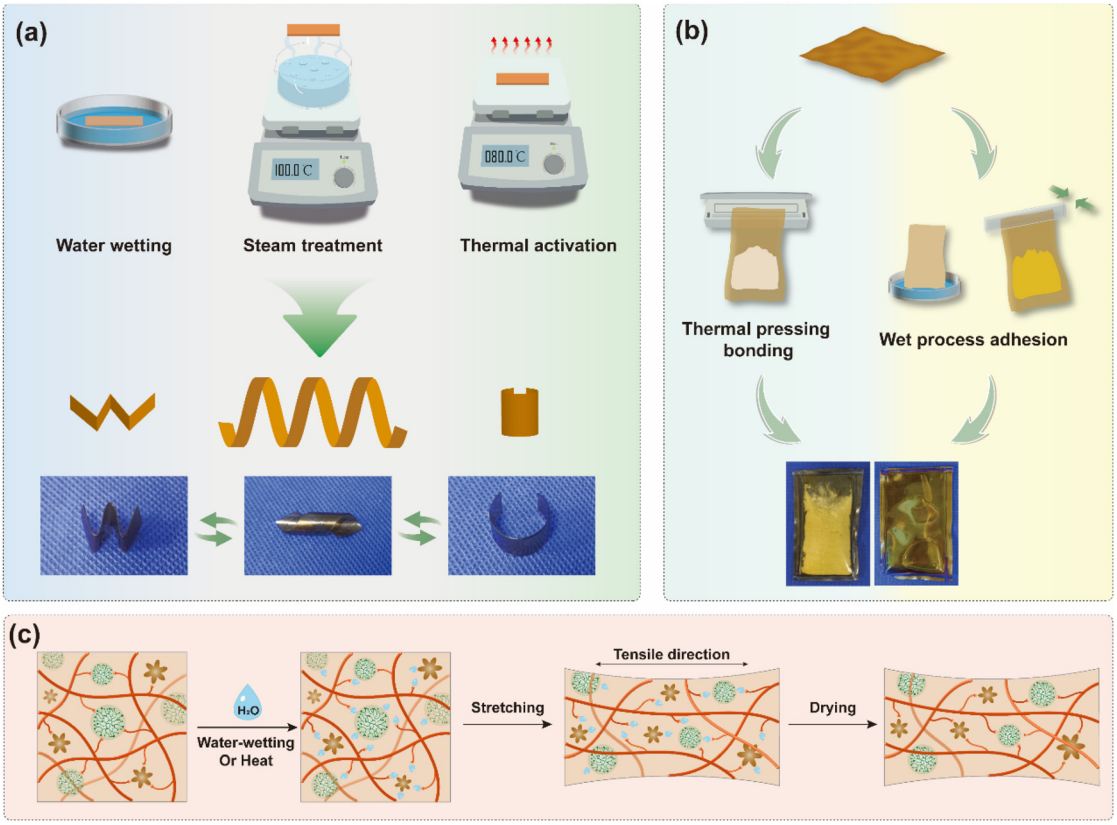

Fig. 6 (a) Demonstration of processability through shape change. (b) Heat sealing and water-assisted bonding of the TP-HBPE-GE film. (c) Schematic of the processing mechanism of the TP-HBPE-GE-5 film.

was then allowed to self-heal using three distinct methods: thermal pressing at 80 °C for 10 min, exposure to water vapor, and water droplet-induced healing. Furthermore, a powder-assisted hot-pressing method was developed to repair large areas of damage. TP-HBPE-GE-5 powder was applied to the damaged regions, followed by thermal compression at 80 °C for 10 min. This enabled complete structural restoration through dynamic bond recombination (Fig. S13).

The closed-loop recyclability of the TP-HBPE-GE films was demonstrated through two regeneration pathways (Fig. 7b): thermal remodeling and aqueous dissolution-recasting. Notably, the latter process enabled the production of multi-functional adhesives with a tunable solid content (Fig. 7c). These adhesives exhibited excellent bonding performance across diverse substrates, achieving 1.21 MPa on wood, where fracture analysis revealed torn and fractured wood fibers combined with interfacial debonding (Fig. S14), and 0.94–0.98 MPa on metallic substrates including copper, aluminium, and steel (Fig. 7d and e). This superior bonding strength originated from synergistic interfacial interactions.[52] Specifically, hydrogen bonds formed between the polar groups of gelatin and the hydroxyl groups of the substrate, electrostatic interactions were mediated by the carboxyl groups on the metal surfaces, and metal chelation was enabled by the catechol moieties in TP with the Cu^{2+}/Al^{3+}. Additionally, cation–π interactions arise from the aromatic rings and the metal cations. Dipole–dipole interactions also arise between the polar groups in the adhesive and the substrate surface. These multimechanistic interactions ensure robust cohesive strength within the adhesive layer and strong interfacial adhesion across diverse substrates (Fig. 7f). Furthermore, the recycled TP-HBPE-GE film solution can be used to form active coatings on the product surfaces *via* dipping or spraying (Fig. 7c). These coatings extend the shelf life by suppressing respiration, oxidative degradation, and microbial growth and can be fully removed by washing in water.

The closed-loop recyclability of the TP-HBPE-GE-5 film enables waste films to be converted into high-value adhesives and coatings. This significantly reduces the environmental footprint through waste-to-resource conversion. End-of-life biodegradation studies revealed that the TP-HBPE-GE film completely biodegraded within 4 weeks of being buried in soil (Fig. S15). During degradation, microbial protease cleaved peptide bonds within gelatin and esterase degraded ester bonds within HBPE. Meanwhile, quinones generated through the oxidation of TP contribute to soil humification by interacting with organic matter.

Taken together, the TP-HBPE-GE film showcases outstanding sustainability throughout its entire life cycle. Its superior processability, self-healing properties, closed-loop recyclability, and environmentally friendly degradation behavior effectively

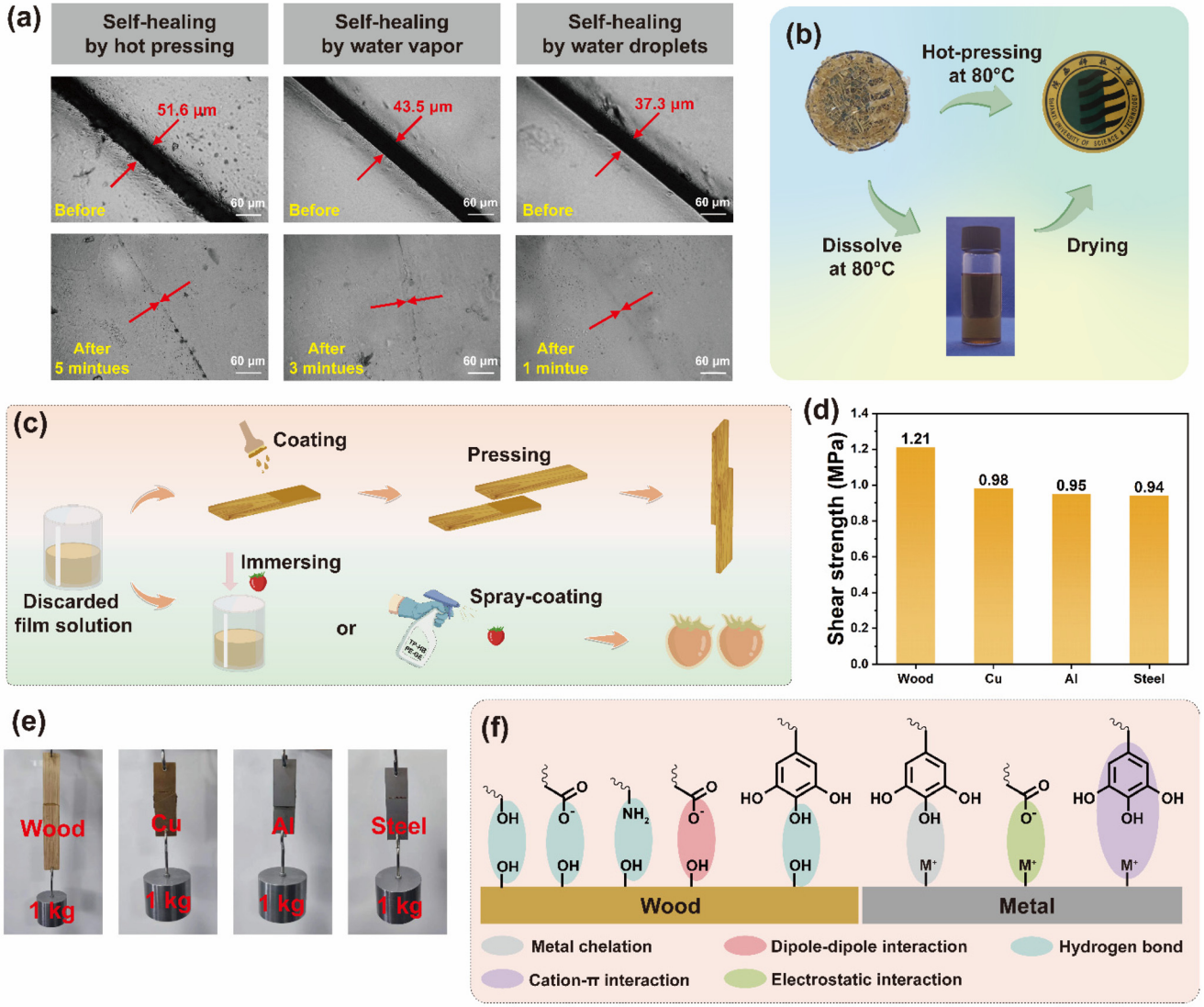

Fig. 7 (a) Super-depth microscopy images of the TP-HBPE-GE-5 bioplastic film before and after self-healing. (b) Schematic of the cyclic regeneration of the TP-HBPE-GE-5 film. (c) Schematic showing the dissolution and regeneration of the bioplastic film after disposal, in order to produce adhesive and active coatings. (d) Adhesion strength and (e) bonding photos of the adhesive prepared from the regenerated TP-HBPE-GE-5 film to different substrates. (f) Adhesion mechanism of the recycled adhesive.

overcome the limitations of conventional plastic films. Multifunctional gelatin-based bioplastic films exhibit sustainability throughout their life cycle by using sustainably sourced biomass-derived raw materials for eco-efficient processing *via* a solution casting technique. The resulting products are circular, with self-repairing functionality, recyclable adhesive and coating applications, and controlled biodegradation. The developed film enhances its economic value and practical applicability and is fully in line with the principles of green chemistry.

4. Conclusion

This study demonstrates a spider web-inspired architectural engineering strategy for developing sustainable gelatin-based bioplastics. The covalent networks formed between HBPE and gelatin provide the essential mechanical robustness, while the dynamic hydrogen bonds and TP-mediated π–π stacking synergistically enable effective stress dissipation, multifunctionality, and processability. The resulting TP-HBPE-GE film achieves tunable mechanical strength and toughness without a glycerol plasticizer, self-healing ability, processability, recyclability, and full biodegradability, thus establishing a closed-loop lifecycle from production to degradation. Notably, its performance in preserving perishable products surpasses that of conventional PVC, highlighting its practical viability. This architecturally engineered bioplastic establishes a sustainable packaging paradigm that directly aligns with core green chemistry objectives: prioritizing renewable resources, minimizing environmental footprints, valorizing waste through closed-loop re-

cycling, and ensuring complete end-of-life biodegradability. It thus provides a compelling solution for replacing petrochemical plastics, simultaneously optimizing critical packaging performance and environmental compatibility.

Conflicts of interest

The authors declare that they have no known competing financial interests or personal relationships that could have appeared to influence the work reported in this paper.

Data availability

The data are available from the corresponding author upon reasonable request.

The Supplementary Information provides additional experimental figures and tables that further support the results reported in this manuscript. Supplementary information is available at DOI: **https://doi.org/10.1039/d5gc02900g**.

Acknowledgements

This work was supported by the National Natural Science Foundation of China (51903144), the China Postdoctoral Science Foundation (2024M752379), and the Doctor's Scientific Subject Foundation of Shaanxi University of Science & Technology (2018QNBJ-05).

References

1 G. Liao, Z. Xiao, X. Chen, C. Du, L. Zhong, C. S. Cheung and H. Gao, *Macromolecules*, 2020, **53**(1), 256–266.
2 J. Cho, B. Kim, T. Kwon, K. Lee and S. Choi, *Green Chem.*, 2023, **25**(21), 8444–8458.
3 J. Zhang, D. Yan, G. Ding, X. Wang, C. Li, S. Zhong, Y. Yu, L. Shuai and G. Liao, *Angew. Chem. Int. Ed.*, 2025, e202511448.
4 Z. Wang, G. Ding, J. Zhang, X. Lv, P. Wang, L. Shuai, C. Li, Y. Ni and G. Liao, *Chem. Commun.*, 2024, **60**(2), 204–207.
5 X. Ma, X. Lin, C. Chang and B. Duan, *ACS Nano*, 2024, **18**(12), 8906–8918.
6 G. Liao, E. Sun, E. B. G. Kana, H. Huang, I. A. Sanusi, P. Qu, H. Jin, J. Liu and L. Shuai, *Carbohydr. Polym.*, 2024, **341**, 122351.
7 Y. Sha, X. Chen, W. Sun, J. Zhou, Y. He, E. Xu, Z. Luo, Y. Zhou and P. Jia, *Nat. Commun.*, 2024, **15**(1), 8480.
8 Z. Wang, Z. Lin, X. Mei, L. Cai, K.-C. Lin, J. F. Rodríguez, Z. Ye, X. S. Parraguez, E. M. Guajardo, P. C. G. Luna, J. Y. J. Zhang and Y. S. Zhang, *Adv. Mater.*, 2025, **36**(14), 2416260.
9 X. Xu, D. Dai, H. Yan, J. Du, Y. Zhang and T. Chen, *Food Chem.*, 2025, **464**, 141895.
10 J. Wen, B. Wang, Y. Xiao, L. Wei, Y. Liu, W. Niu, H. Wang, H. Yan, B. Niu and W. Li, *Chem. Eng. J.*, 2025, **511**, 161638.
11 J. Kumankuma-Sarpong, C. Chang, J. Hao, T. Li, X. Deng, C. Han and B. Li, *Adv. Mater.*, 2024, **36**(30), 2403214.
12 C. Shen and X. Liu, *Science*, 2024, **385**(6704), 30.
13 F. Abookleesh, M. Zubair and A. Ullah, *Chem. Eng. J.*, 2025, **512**, 162604.
14 L. Chen, T. Qiang, W. Ren, Q. Tian, X. Zhang and H. J. Zhang, *J. Cleaner Prod.*, 2023, **385**, 135705.
15 B. Guo, G. Liu, W. Ye, Z. Xu, W. Li, J. Zhuang, X. Zhang, L. Wang, B. Lei, C. Hu, Y. Liu and H. Dong, *Food Hydrocolloids*, 2024, **147**, 109327.
16 H. Cui, Q. Cheng, C. Li, M. N. Khin and L. Lin, *Food Hydrocolloids*, 2023, **141**, 108744.
17 Y. Guo, Z. Chang, B. Li, Z.-L. Zhao, H.-P. Zhao, X.-Q. Feng and H. Gao, *Appl. Phys. Lett.*, 2018, **113**(10), 103701.
18 J. H. Kim, K. S. Song, Y. Kim, J. Y. Cho, K. Lee, D. G. Lee, J. H. Jin, J. Kim, J. H. Park, W. H. Lee, T. Kim and J. T. Han, *ACS Nano*, 2025, **19**(4), 4601–4610.
19 S. Hong, J. Lee, T. Park, J. Jeong, J. Lee, H. Joo, J. C. Mesa, C. B. Alston, Y. Ji, S. R. Vega, C. Barinaga, J. Yi, Y. Lee, J. Kim, K. J. Won, L. Solorio, Y. L. Kim, H. Lee, D. R. Kim and C. H. Lee, *Adv. Sci.*, 2025, **12**(12), 2500397.
20 A. D. Malay, N. A. Oktaviani, J. Chen and K. Numata, *Adv. Funct. Mater.*, 2025, **35**(15), 2408175.
21 Y. Jiang, J. Li, D. Li, Y. Ma, S. Zhou, Y. Wang and D. Zhang, *Chem. Soc. Rev.*, 2024, **53**(2), 624–655.
22 J. Zhang, Z. Gong, C. Wu, T. Li, Y. Tang, J. Wu, C. Jiang, M. Miao and D. Zhang, *Green Chem.*, 2022, **24**(18), 6900–6911.
23 J. Zhang, C. Jiang, G. Deng, M. Luo, B. Ye, H. Zhang, M. Miao, T. Li and D. Zhang, *Nat. Commun.*, 2024, **15**(1), 4869.
24 J. Ma, Z. Du, S. Gao and J. Zang, *Trends Food Sci. Technol.*, 2024, **146**, 104665.
25 R. Zhao, H. Qian, X. Zhu, X. Zhang, Z. Chen and X. Yang, *Adv. Funct. Mater.*, 2024, **34**(32), 2401566.
26 Y. Wang, X. Guo, Z. Qin, R. Liu, S. Li, M. Du, S. Qiu and Y. Bai, *Food Packag. Shelf Life*, 2025, **49**, 101482.
27 X. Chen, Z. Liu, W. Ma, H. Wang, Q. Dong and L. Li, *Food Hydrocolloids*, 2024, **151**, 109769.
28 Q. Wang, S. Yan, Y. Zhu, Y. Ning, T. Chen, Y. Yang, B. Qi, Y. Huang and Y. Li, *Food Chem.*, 2024, **456**, 140090.
29 Y. Liu, Y. Zhang, M. Zhen, Y. Wu, M. Ma, Y. Cheng and Y. Jin, *Food Hydrocolloids*, 2023, **135**, 108141.
30 X. Dang, Y. Du and X. Wang, *Food Chem.*, 2024, **439**, 138119.
31 M. Wei, M. Shan, L. Zhang, N. Chen, H. Tie, Y. Xiao and Z. Li, *Food Hydrocolloids*, 2024, **153**, 110023.
32 L. Chen, T. Qiang, X. Chen, W. Ren and H. J. Zhang, *Waste Manag.*, 2022, **145**, 10–19.
33 K. Yu, L. Zhou, H. Huang, J. Xu, Y. Li, W. Yu, S. Peng, L. Zou and W. Liu, *Food Chem.*, 2024, **450**, 139352.
34 F. Sun, J. Zhao, P. Shan, K. Wang, H. Li and L. Peng, *Food Hydrocolloids*, 2025, **159**, 110610.

35 H. Montazerian, R. R. Sampath, N. Annabi, A. Khademhosseini and P. S. Weiss, *Acc. Mater. Res.*, 2023, **4**(7), 627–640.
36 J. Ren, Y. Li, Q. Lin, Z. Li and G. Zhang, *Int. J. Biol. Macromol.*, 2022, **217**, 814–823.
37 Q. Tong, Y. Xiao, Z. Yi, X. Chen, X. Jiang and X. Li, *Green Chem.*, 2023, **25**(11), 4387–4401.
38 T. Luo, Y. Sha, Y. Bei, Z. Meng, Y. Hu, M. Zhang, Y. Zhou and P. Jia, *Chem. Eng. J.*, 2025, **526**, 164629.
39 Z. Chang, Y. Shen, J. Xue, Y. Sun and S. Zhang, *Chem. Eng. J.*, 2023, **457**, 140984.
40 Z. Qiao, Y. Chen, H. Pan, J. Li, Q. Meng, J. Wang, Y. Cao, W. Wang and Y. Yang, *Int. J. Biol. Macromol.*, 2024, **282**, 137219.
41 D. Gao, H. Wu, B. Lyu, X. Lu and J. Ma, *Int. J. Biol. Macromol.*, 2025, **284**, 138165.
42 T. Qiang, W. Ren and L. Chen, *Food Hydrocolloids*, 2024, **149**, 109539.
43 Z. Rashedi, R. Mawhinney, W. Gao, A. Salaghi and P. Fatehi, *Carbohydr. Polym.*, 2025, **350**, 123044.
44 J. Li, W. Liu, A. Chang, Z. Foudeh, J. Yu, P. Wei, K. Chen, C. Hu, P. Dhatt, S. Y. Dai and J. S. Yuan, *Green Chem.*, 2025, **27**(18), 5104–5118.
45 M. Yang, T. Wang, Y. Tian, H. Zhang, J. Zhang and J. Cheng, *Green Chem.*, 2024, **26**(8), 4771–4784.
46 Y. Li, B. Yuan, S. Yu, Z. Xia, Y. Nishiyama, P. Chen, W. Li and M. Liang, *Food Hydrocolloids*, 2024, **156**, 110296.
47 F. Li, S. Mao, Y. Xu, L. Pan, W. Wang, T. Zhang and C. Lu, *Food Chem.*, 2025, **488**, 144086.
48 W. Zhang, M. Li, J. Chen, Y. Chen, C. Liu and X. Wu, *J. Agric. Food Chem.*, 2024, **72**(38), 20705–20721.
49 X. Han, Q. Wang, J. Mi, J. Zhang, J. Feng, T. Du, L. Luo, C. Zhang, J. Wang and W. Zhang, *Chem. Eng. J.*, 2025, **521**, 160420.
50 H. Jin, G. Sun, Q. Tang, S. Wang, S. Liu, Q. Cheng, L. Wang and Y. Li, *Carbohydr. Polym.*, 2025, **353**, 123306.
51 Z. Zeng, L. Yu, S. Yang, K. Guo, C. Xu, C. Chen and Z. Wang, *Matter*, 2024, **7**(9), 3036–3052.
52 Y. Hu, Y. Sha, Y. Fang, M. Zhang, Y. Zhou, P. Jia and T. Zhu, *Cell Rep. Phys. Sci.*, 2025, **6**(5), 101768.